Research Article

Intracellular trafficking of a human dynein light chain T-Rp3-containing non-viral gene therapy vector.

Marianna Teixeira de Pinho Favaro[1,2]; Ugutz Unzueta[3,4]; Martí de Cabo[5]; Antonio Villaverde[1,6,4]; Adriano Rodrigues Azzoni[7]; Neus Ferrer-Miralles[1,6,4]

[1]Institut de Biotecnologia i de Biomedicina, Universitat Autònoma de Barcelona, Bellaterra, 08193 Barcelona, Spain.
[2]Centro de Biologia Molecular e Engenharia Genética, Universidade Estadual de Campinas, Av Candido Rondon, 400, 13083-875 Campinas, SP, Brazil.
[3]Oncogenesis and Antitumor Drug Group, Biomedical Research Institute Sant Pau (IIB-SantPau), Hospital de la Santa Creu i Sant Pau, 08025 Barcelona, Spain.
[4]CIBER de Bioingeniería, Biomateriales y Nanomedicina (CIBER-BBN), Bellaterra, 08193 Barcelona, Spain.
[5]Servei de Microscòpia, Universitat Autònoma de Barcelona, Bellaterra, 08193 Barcelona, Spain.
[6]Departament de Genètica i de Microbiologia, Universitat Autònoma de Barcelona, Bellaterra, 08193 Barcelona, Spain.
[7]Departamento de Engenharia Química, Escola Politécnica, Universidade de São Paulo, Av. Prof. Luciano Gualberto, Trav. 3, Nº 380, 05508-900 São Paulo, SP, Brazil.

Keywords: gene delivery; intracellular trafficking; non-viral gene therapy; dynein molecular motor; recombinant modular protein.

Abbreviations: MTOC, microtubule organizing center; **MES**, 4-Morpholineethanesulfonic acid hydrate (pH 6.0); **TEM**, Transmission electron microscopy; **DLS**, dynamic light scattering; **LSCM**, laser scanning confocal microscopy.

ABSTRACT

Non-viral gene therapy is often proposed as an alternative to viral gene therapy, which is widely associated to safety concerns and elevated production costs. However, non-viral vectors suffer from limited transfection efficiency. The success of viruses in the delivery of the viral genome to target cells relies on the evolutionary selection of protein-based domains able to hijack the intermolecular interactions through which cells respond to intra- and extracellular stimuli. In an effort to mimic viral transfection capabilities, a modular recombinant protein named T-Rp3 was recently developed, containing a DNA binding domain, a dynein molecular motor interacting domain, and a TAT-derived transduction domain. Here, we analyzed at the microscopic level the mechanisms behind the cell internalization and intracellular trafficking of this efficient modular protein vector. We found that the protein has the ability to self-assemble in discrete protein nanoparticles resembling viral capsids, to bind and condense plasmid DNA (pDNA), and to interact with eukaryotic cell membranes. Confocal and single particle tracking assays performed on living HeLa cells revealed that the T-Rp3 vector promoted an impressive speed of cellular uptake and perinuclear accumulation, mainly due to interaction with microtubules and fast translocation towards the microtubule organizing center (MTOC). Finally, the protein demonstrated to be a versatile vector, delivering siRNA at efficiencies comparable to Lipofectamine™. The results presented here demonstrate the high potential of recombinant modular proteins with merging biological functions to fulfill several requirements needed to obtain cost-effective non-viral vectors for gene-based therapies through the rational design of proteins formulated with the desired therapeutic nucleic acid.

1 INTRODUCTION

Since the first gene therapy trial in 1990, more than 2,000 trials have been approved (http://www.abedia.com/wiley/). However, despite the great efforts made towards the development of gene therapies to replace faulty or missing genetic material in patient's DNA, no single commercial product has been yet approved by the Food and Drug Administration (FDA) and only one has been granted by the European Medicines Agency (EMA) under the trade name Glybera (alipogen tiparvovec) [1,2]. Glybera is based on a non-replicating adeno-associated virus designed to deliver a functional gene copy of the lipoprotein lipase gene. [3]. Other research products will probably be granted in the years to come provided preliminary data reveal their effectivity (Lentiglobin BB305 lentiviral vector, for instance) [4]. However, viral vectors are difficult to produce and purify at large scale. In addition, immunosuppression regimes have to be administered prior to the gene therapy treatment and their administration for a therapeutic approach entails environmental risks involved in using genetically modified replicative entities (Baldo et al., 2013; Clement et al, 2010; Mingozzi and High, 2016).

In this scenario, novel non-viral gene delivery strategies have been explored to deliver therapeutic nucleic acids. These vectors have to be designed to display the three basic characteristics of viral gene therapy vectors: 1) a potent nucleic acid packaging capability; 2) the ability to overcome physiological barriers upon administration; and 3) effective cellular uptake and sub-cellular interactions [8]. As low transfection efficiency is the limiting factor of non-viral gene therapy vectors, the biological barriers involved in that process have to be analyzed in detail. Those include the plasma membrane with a plethora of internalization mechanisms governing the cellular homeostasis. In this sense, the size of the vehicle is of great relevance, being optimal between 30-50 nm [9,10] for rigid spherical particles, although cell internalization has been demonstrated for nanoparticles up to 200

nm [11]. On the other hand, when this first barrier is overcome, the loaded endosomes have to face the fusion of lysosomes which often leads to the degradation of the vehicle and the cargo. Several viral-inspired peptides can be then included in the design of the vehicle to escape from this hurdle. At that time, if the cargo is intended to perform its function in the cytoplasm, no more biological barriers are encountered. However, if nucleus is the targeted cellular compartment, the presence of a nuclear localization signal may improve efficiency. Taking into account those considerations a novel generation of non-viral vectors is now under study, gaining attention for its performance in pre-clinical studies. Among the different types of delivery vehicles which can be decorated with functional moieties, recombinant proteins appear as a promising alternative due to the versatility in their design [12]. Being biocompatible molecules, proteins offer an almost infinite platform to obtain gene therapy vehicles with regulatable immunogenicity, adequate nanoscale size and specific functionalization. In addition, their production can be scaled up in cost effective expression systems from which they can be easily purified. In this context, we have designed a protein-based gene-therapy delivery vector by the thorough selection of four sequential functional domains. The N-terminal His-tag provides an endosomal escape moiety and also serves as an efficient purification tag [13]. The DNA-binding domain allows binding and condensation of expressible DNA for the formulation of the vector [14]. The third element is the human dynein light chain Rp3 [15]. Dyneins are motor-containing protein complexes formed by a heavy chain polypeptide interacting with several associated subunits that directly or indirectly load cargoes to be transported towards the microtubule organizing center (MTOC) [16]. The addition of Rp3 is expected to improve the intracellular movement of the vehicle towards the nucleus. Finally, a TAT inspired domain confers cell penetrating properties to the vehicle type [17]. TAT is a transcriptional transactivator of HIV which has been demonstrated to enter the cell via different mechanisms, which largely depend on the type of attached cargo and cell type [18–20]. In this work, the mechanisms behind the cell

uptake and intracellular trafficking of the modular protein vector T-Rp3 are further analyzed. The ability to mimic viral infection capabilities is demonstrated at the microscopic level. Furthermore, the vector shown to be able to efficiently delivery not only large pDNA cargos, but also the much smaller siRNA molecules. This type of tuned and versatile recombinant protein is envisioned as a powerful alternative to the viral vectors for gene-therapy purposes.

2 MATERIALS AND METHODS

2.1 Recombinant protein production

The recombinant T-Rp3 was expressed in *E. coli* BL21 (DE3) and purified by a single step Ni-chelating affinity chromatography in an ÄKTA purifier FPLC (GE Healthcare) as previously described [20]. Protein was then dialyzed against 50 mM MES buffer (4-Morpholineethanesulfonic acid hydrate) (pH 6.0) overnight at room temperature, frozen in liquid nitrogen and stored at -80 ºC after filtration through 0.22 µm pore membrane.

2.2 Evaluation of DNA-protein interaction by Electrophoretic Mobility Shift Assay (EMSA)

Protein-DNA complexes were formed using 1 µg of pTriEx-1.1 Hygro plasmid (Novagen) at different pDNA: protein molar ratios (1:100, 1:200, 1:500, 1:1000, 1:2000, 1:8000) during 10 minutes in a final volume of 50 µL in 50 mM MES buffer pH 6.0. The increasing molar ratios were assessed by EMSA assay on a 0.8% agarose gel and visualized by ethidium bromide staining. For further experiments, all samples were prepared at 1:8000 pDNA:protein molar ratio with 1 µg of pDNA and the corresponding amount of protein as described above.

2.3 Transmission Electron Microscopy (TEM)

Droplets of each sample (0.05 mg/mL or 0.1 mg/mL of protein, with or without pDNA) were deposited onto a carbon-coated copper grid for 5 min, and excess specimen was dried out with filter paper. Samples were submitted to negative staining with uranyl acetate and observed with a Jeol JEM 1400 transmission electron microscope, equipped with a CCD Gatan ES1000W Erlangshen camera.

2.4 Dynamic Light Scattering

Volume size distribution of protein nanoparticles and pDNA:protein complexes were measured using a dynamic light scattering (DLS) analyzer at a wavelength of 633 nm (Zetasizer Nano ZS, Malvern Instruments Limited). Samples were prepared as previously described for EMSA assays, where the corresponding amount of each molar ratio of protein is added to 1μg pDNA in a final volume of 50 μL in 50 mM MES buffer pH 6.0. Samples were incubated for 10 minutes, placed in the cuvette and measured at 25 ºC in triplicate, corresponding approximately to 10 minutes readings.

2.5 Cell culture and laser scanning confocal microscopy (LSCM)

HeLa cells were cultured in MEMα Glutamax (Gibco) supplemented with 10% fetal calf serum (Gibco), and incubated at 37 ºC and 5 % CO2 in a humidified atmosphere. For LSCM imaging, cells were grown on MatTek culture dishes (MatTek Corporation). The nuclei were labeled with 5 μg/mL Hoechst 33342 (Molecular Probes), lysosomes were labeled with 200 nM LysoTracker® Red (Molecular Probes), and the plasma membranes with 5μg/mL CellMask™ Deep Red (Molecular Probes) for 15 minutes in dark. The cells were then washed in phosphate-buffered saline (Sigma-Aldrich Chemie GmbH). Live cells were

recorded by TCS LSCM (Leica Microsystems) equipped with Argon 488, DPSS 561, HeNe 633 and Diode 405 lasers for the excitation of GFP and Atto 488 (Sigma Aldrich), LysoTracker and CellMask, Draq5 and Hoechst 3342, respectively. A Plan Apo 63 × /1.4 (oil HC × PL APO lambda blue) objective was used. To determine the localization of engulfed particles inside the cell, 0.29 μm sections were acquired and three-dimensional models were generated using Imaris 7.3.0 version software (Bitplane). The protein was labeled with Atto 488 according to manufacturer´s protocol and the plasmid was labeled with Draq5 (Thermo Scientific) ahead of transfection, which resulted in mild labeling of the nuclei. In order to visualize microtubules, HeLa cells were prepared as described and transfected 24 hours before microscopy imaging with pAcGFP1-Tubulin (Clontech) using Lipofectamine LTX (Invitrogen). pDNA:protein complexes were prepared as described above and added to complete-media-containing cell culture, and images were then taken 30 to 60 minutes after transfection.

2.6 Transfection of HeLa cells

For transfection assays, HeLa cells were transfected with pDNA T-Rp3 in the molar ratio 1:8000 using GFP as reporter gene. Protein-DNA complexes were formed in 50 μL in 50 mM MES buffer pH 6.0 for 10 minutes. The mixture was the added to 24 well plates containing 250 μL Optipro medium (Gibco) with cells at 70% confluency.Chloroquine 100 μM was added 2 hours pre-transfection in the presence of Optipro medium (Gibco). Control experiments were performed in the same conditions but without the addition of chloroquine. The medium was replaced 6 hours post-transfection and cell samples were analyzed 24 hours post-transfection after treatment with 1 mg/mL trypsin (Gibco) for 15 minutes on a FACSCanto system (Becton Dickinson) using a 15 mW air-cooled argon ion laser at 488 nm excitation. Fluorescence emission was measured with a D detector (530/30 nm band pass filter).

2.7 Single Particle Tracking using FIJI (Image J)

HeLa cells were grown as described for LSCM analysis. T-Rp3 labeled with Atto 488 was incubated with unlabeled pDNA for 10 minutes and then added to cell culture. 5 minutes later, the plasma membrane was labeled with 5 μg/mL CellMaskTM Deep Red (Molecular Probes) and the nuclei were labeled with 5 μg/mL Hoechst 33342 (Molecular Probes) for 10 minutes before being washed in phosphate-buffered saline. Live cells were recorded by TCS-SP5 LSCM (Leica Microsystems) by taking images every 2 seconds for 5 minutes. Manual particle tracking was performed on FIJI distribution package [21] for 4 fast-moving particles.

2.8 Gene silencing through iRNA

For siRNA assays we used the luciferase system in HeLa cells, with single-stranded RNA sequences targeting the luciferase GL3 gene (Elbashir et al., 2001) (5'-CUUACGCUGAGUACUUCGATT-3' and 3' – TTGAAUGCGACUCAUGAAGCU – 5') synthesized (Sigma-Aldrich), solubilized in UltraPure DEPC-treated water to 1 mM and diluted to 40 μM in annealing buffer (100 mM potassium acetate, 30 mM HEPES-KOH, 2 mM magnesium acetate; pH 7.4, DEPC-treated). Complementary strands were annealed for one minute at 90˚C, followed by one hour at 37˚C in a PTC-200 Peltier Thermal Cycler. For the assay HeLa cells were transfected with 1μg/well of pVAX-LUC plasmid containing Luciferase gene (Toledo et al., 2012) using Lipofectamine™ 2000 (Invitrogen) as transfection reagent, according to the manufacturer instructions. After 5 hours of incubation at 37 °C in 5% CO2 humidified environment, the medium was replaced and cells were transfected with 40 or 100 nM luciferase targeting dsRNA, using T-Rp3 or Lipofectamine™ 2000 as control transfecting reagent (following manufacturer instructions). Cells were further incubated for

6 hours at 37 °C in 5% CO2 humidified environment before the medium was replaced, and 24 hours after the first transfection cells were collected and analyzed for luciferase activity using the Luciferase Assay System (Promega), following the manufacturer's instructions. Luminescence intensity was normalized by total protein concentration in each sample, which was determined with a Micro BCA Protein Assay Kit (Thermo Scientific). All assays were performed in triplicate.

3 Results and Discussion

3.1 Characterization of T-Rp3-DNA complexes

T-Rp3 is a modular recombinant protein based on dynein light chain Rp3, to which a DNA binding domain, a histidine tag and a TAT peptide was added as previously described (Fig. 1A) [20]. This protein had been shown to efficiently transfect HeLa cells in a process dependent of the microtubule network, although the mechanism by which it takes place was still not unraveled [20]. The T-Rp3 protein used in this study was produced in *E. coli* and successfully purified by a single-step affinity chromatography. Through coomassie blue staining and western blot analysis using anti-his primary antibody, the recombinant protein was identified as a single band with no significant contaminant protein bands (Fig. 1B). The purified protein has a DNA-binding domain responsible for interacting with pDNA, thus different pDNA:protein molar ratios were used to induce the formation of complexes that were further analyzed by EMSA (Fig. 1C), indicating that at 1:500 molar ratio most of the pDNA is complexed with the protein. Since in previous reports the plasmid used had 4450 bp [20], we evaluated here the protein's capacity to equally condensate a larger plasmid, of 6951bp. The pDNA was complexed to the protein at similar molar ratios, hence indicating that T-Rp3 capacity to interact with pDNA is maintained for larger plasmids. The effect of pDNA:protein molar ratios on the size and polydispersity of the generated nanoparticle was

also evaluated, using dynamic light scattering (Fig. 1D-I). As molar ratio increase, the complex's size also increases, as well as the polydispersity, reaching over 900 nm at 1:500 molar ratio, with a polydispersity index of 0.246 at this ratio. With the further addition of protein, the particle's size begins to decrease at 1:1000, reaching 147.5 nm at 1:8000 molar ratio, with lower polydispersity (0.125). Since the protein is positively charged, it binds to pDNA resulting in an increase of size up to the neutrality point, after which the condensation process begins, leading to a reduction in size. Even though we had previously observed that the increase in the molar ratio positively impacts the transfection efficiency, until now we had been not able to correlate the internalization with the characteristics of the resulting nanoparticle formed at different ratios. For further experiments, the 1:8000 molar ratio was used, as this is the condition in which the protein-DNA complexes were the smallest and the higher transfection efficiency achieved [20].

The protein alone as well as the complex formed by the protein with pDNA, were evaluated by transmission electron microscopy for the first time. Our previous findings using DLS measurements of the protein alone in solution consistently presented a high polydispersity index. However, the images obtained now using TEM show that T-Rp3 presents the capacity to self assemble in small nanoparticles of toroidal shape (Fig. 2A-C), while some aggregates are also visible. In the presence of pDNA (Fig. 2D-F) we observed larger nanoparticles of a globular shape. Consistent with TEM images, DLS assays (Fig. 2G) indicated that protein alone forms nanoparticles of less than 10 nm, with a higher polydispersity, which is reduced in the presence of pDNA. This result was consistent with AFM images of Lc8-based protein interacting with pDNA [14]. A large number of proteins involved in DNA metabolism assume a toroidal structure, and this ring-shaped conformation is believed to facilitate the topological link to DNA [22]. Even protamine, a protein associated to DNA condensation in spermatogenesis and occasionally used as a gene delivery vector, forms toroid-shaped nanoparticles. This new evidence indicateed that the

modular approach used to build the recombinant T-Rp3 allowed the development of a protein with self assembling capacity that mimics the toroidal conformation widely used in nature for DNA-binding. For instance, Western blotting analysis of extracts from Hela cell submitted to T-Rp3 protein (alone), T-Rp3-DNA, and T-Rp3-dsRNA transfection indicated that internalization occurs in all cases (data not shown), pointing to the versatility of uses of this modular vector.

3.2 Intracellular trafficking of T-Rp3-DNA complexes

Previous confocal microscopy images obtained for T-Rp3-DNA internalization gave indications that it could accumulate in the perinuclear region, in a pattern that differs from that of other delivery proteins, such as protamine [20]. However, those experiments were performed with fixed cells, and it is now well established that the fixation of cells may alter the internalization process, which is especially significant for cell penetrating peptides [Takeuchi and Futaki 2016]. For the aim of this study, LSCM imaging was performed on live HeLa cells, and for the first time the protein itself was fluorescently labeled, as well as the pDNA. Considering that size is regarded as an important feature affecting transfection efficiency, protein-DNA complexes formed with Atto 488-stained protein and DRAQ5-stained plasmid were evaluated by dynamic light scattering and transmission electron microscopy. Results reveal that Atto 488 can promote a slight decrease in complex size, but the presence of Draq5 did not alter its size (Fig. 1 supplementary material). However, the presence of stain does not impair the formation of nanoparticles, as can be observed by TEM.

A previous report suggested that T-Rp3 depends on microtubules network to accomplish gene delivery [20], although this hypothesis was still not confirmed by live particle tracking. In an attempt to better understand the intracellular trafficking mediated by T-Rp3 vector, the protein was previously stained with Atto 488 to evaluate the kinetics

entrance in living HeLa cells. Images shown at Fig.3A indicated an accumulation of T-Rp3 (in green) in a well-defined region in perinuclear area as soon as 30 minutes post-transfection. This was consistent with delivery through microtubule since MTOC was usually located close to the cell nucleus [23]. Three-dimensional isosurface reconstructions from LSCM stack images of transfected cells (Fig. 3B-C) showed that the protein was actually located inside the cell, and occasionally trapped to nuclear membrane, with a small portion of it embedded in the nucleus. In the single particle tracking video supplied in supplementary material (video 1), the protein is stained in green and can be observed concentrated around the cells as soon as 15 minutes after being added to the medium, thus confirming how fast the internalization process takes place.

Aiming to determine if the microtubule transport occurs by direct interaction of T-Rp3 with dynein or if the accumulation is due to complexes transported inside endosomes, pDNA (stained with Draq5, seen in blue), T-Rp3 (stained with Atto488, in green) and late endosomes/lysosomes (stained with LysotrackerRed, in red) were observed inside live HeLa cells 30 minutes post transfection, when perinuclear accumulation was previously observed. Isosurface reconstructions indicated that all arrangements were present (Fig. 4A), detecting free pDNA:T-Rp3 particles as well as trapped nanoparticles inside lysosomes. Non-complexed protein and pDNA-only particles were also observed. Sections of isosurface reconstructions (Fig. 4B-C) demonstrated the association of pDNA with T-Rp3 in protein nanoparticles contained in lysosomes or free in the cytosol. These results suggest that although part of the pDNA:T-Rp3 particles are retained inside endosomes, another part may be free to directly interact with molecular motors. As entrapment in acidic lysosomal compartments reduces transfection efficiency of gene therapy vectors, the detection of free pDNA:T-Rp3 particles might have a positive impact in this parameter [24]. For a more complete representation, please refer to the video 2 supplied in supplementary information. The fast perinuclear accumulation may be a result of an active transport being particles

directly interacting with dynein, as well as travelling inside endo/lysosomes. Protamine-containing nanoparticles which were entrapped in lysosomes, for instance, take up to 12 hours to be internalized *in vitro* [25]. Unlike in previous experiments, in this case the fast internalization of T-Rp3 complexes could be followed in live cells using shorter incubation times.

3.3 Tracking T-Rp3-DNA complexes movement along microtubules

In order to analyze the effect of the endosomal entrapment of T-Rp3 nanoparticles, transfection experiments were performed in the presence of chloroquine, which is known to prevent lysosomal degradation due to acidification. In that case, transfection efficiency was increased from 15% to 23%, thus indicating that some particles actually remain trapped in endosomes (data not shown). To further evaluate microtubule participation in the traffic of T-Rp3 particles, HeLa cells were transfected with pAcGFP1-Tubulin 24 hours before microscopy so that microtubules could be observed in green. These cells were transfected with unstained T-Rp3 using pDNA previously stained with Draq5. As early as 30 minutes post-transfection, most plasmids could be observed nearby microtubules (Fig. 5A). While most red dots are seen on green filaments, areas with no filaments tend to be plasmid-free.

Since naked pDNA poorly diffuses through cytoplasm [26–28], evaluating the particle speed inside the cell is an important indication of whether microtubule network is involved. Single particle tracking assays were performed on living HeLa cells, although the experiment was limited by the great speed of perinuclear accumulation, which restricted the use of 3D imaging in this case. On Fig. 5B, green dots representing pDNA:T-Rp3 are observed 15-30 minutes post transfection distributed inside the cell as well as attached to the cell membrane, as yellow dots indicates that the protein is embedded in cell membrane. Fig. 5C is a still from the video supplied in the online version of this article (Video 3,

supplementary). The video is a 5-minutes-long particle tracking captured 30 minutes post-transfection where particles move inside the cell in high speed, in linear displacements that stop and go, bidirectionally. From the video, four particles were manually tracked and their trajectories are highlighted in colors (the pink and the blue trails can be partially seen in the Fig. 5C), their speed being thus calculated and plotted (Fig. 5D). The speed varies along time, indicating that T-Rp3 is capable of exploiting microtubules in a similar approach to viruses, that also stop-and-go along microtubules [23].

Surprisingly, single particle tracking images revealed a bidirectional movement (Video 3 in supplementary material) which was also observed for viruses that exploit this strategy to move along microtubules [29,30]. To the best of our knowledge, this is the first report of a non viral vector that mimics this viral strategy to this extent. *In vitro* evaluation of molecular motors' behavior when facing a microtubule intersection elucidated that dynein can overpass the intersection, move to another filament, and also reverse movement towards plus-end of microtubules, with an expected speed of 980 ± 70 nm/s for dyneins and 560 ± 30 nm/s for kinesins on nonintersecting microtubules [31]. The expected speed for dynein is compatible to the one observed for T-Rp3 particles (Fig. 5D), indicating that T-Rp3 is capable of exploring molecular motors to accomplish intracellular trafficking. In previous experiments, the velocity of similar non-viral vectors whithout a dynein binding domain in transfection experiments had been calculated as 4.4 ± 0.3 nm/s, indicating an improvement in intracellular shuttle in the presence of such domain [32]. For polyplexes moving inside vesicles previous studies found an average speed of 0,19 μm/s [33]. Although dyneins essentially move towards the minus end of microtubules, previous reports indicate that about 30 % of dynein-dynactin runs are directed toward the plus ends of polarity-marked microtubules [34]. T-Rp3 has already been reported to be highly dependent on microtubules to achieve efficient gene delivery, with transfection efficiency being reduced in 92 % in the presence of nocodazole, a microtubule depolymerizing agent [20]. These

assays now reveal that pDNA:T-Rp3 particles are preferentially associated to microtubules and use the molecular motors to achieve high speed intracellular trafficking, thus efficiently mimicking viral particles that exploit microtubules to perform fast and bidirectional movement in a stop-and-go pattern.

3.4 Delivery of dsRNA to Hela cells

With the broadening of oligonucleotide-based approaches used in gene delivery assays, promising vectors are expected to have expanded capabilities as well. Since T-Rp3 has previously shown to efficiently delivery plasmid DNA to HeLa cells, we evaluated the ability of this vector to delivery dsRNA, to be used in gene silencing experiments. Confirming previous Western blotting analysis that indicated cellular uptake of T-Rp3-dsRNA complexes, the results presented in Figure 6 show that T-Rp3 can achieve a performance in Luciferase silencing similar to that of the commercial lipid Lipofectamine™ 2000. Even though Lipofectamine™ 2000 is associated with high toxicity, it can still be considered a golden standard for transfection efficiency. Although the cytotoxicity of the T-Rp3-dsRNAi complexes were not assessed here, these results points to the versatile of this modular protein, presenting the ability to fast and efficiently delivery different nucleic acids cargos to cultured HeLa cells.

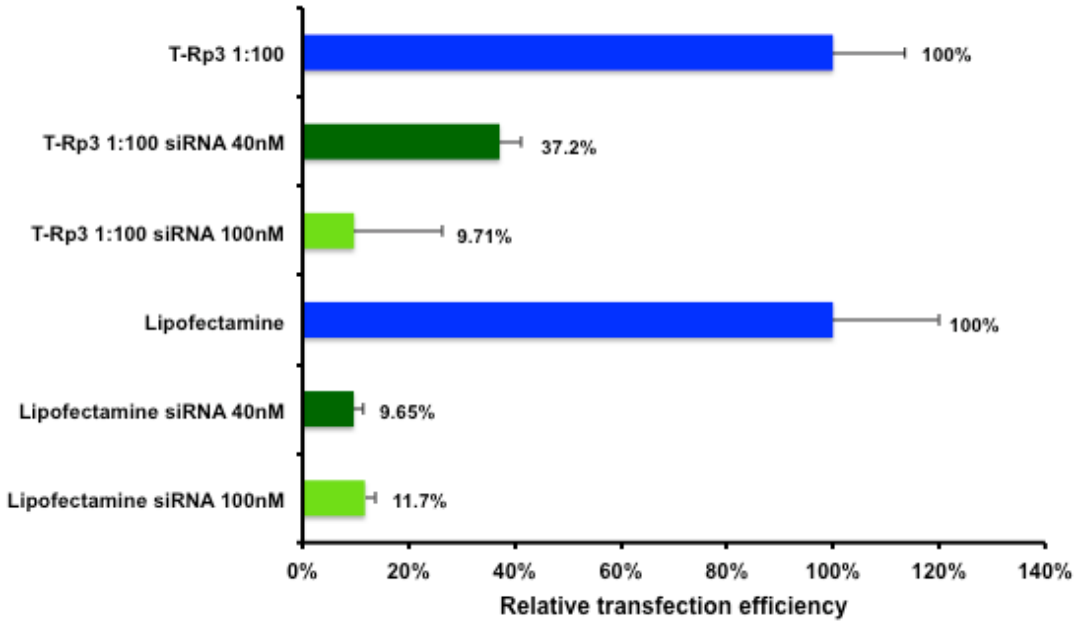

Figure 6: Gene silencing of Luciferase expression in HeLa cells achieved by the delivery of 40 and 100 nM dsRNA by either T-Rp3 or Lipofectamine™ 2000.

4 Conclusions

Engineering modular recombinant proteins is a feasible approach to address the several steps involved in protein internalization for gene delivery. Considering that viruses successfully exploit microtubule network, addressing this step may lead to nanoscale vectors that better mimic the viral counterparts. Physicochemical characterization of modular T-Rp3 protein alone showed for the first time the presence of toroidal structures that are observed in naturally-occurring DNA-interacting proteins, thus indicating how tunable proteins can be. In addition, T-Rp3 had been reported to efficiently transfect HeLa cells with low toxicity, but the extent of microtubule involvement remained unexplored and poorly characterized. Here, transfected live cells were analyzed by laser scanning confocal microscopy. The results indicate that T-Rp3 nanoparticles behave as fast-transfecting vectors that bind to cell membrane within minutes, and are further internalized to accumulate in localized regions of cytoplasm. In less than one hour, particles are already

trapped to nuclear membrane, in a process much faster than other protein-based delivery vehicles. Single particle tracking finally reveals that T-Rp3 not only is closely associated to microtubule in LSCM images, but also moves inside the cell with a motion pattern and speed compatible with a direct microtubule interaction, in a movement similar to those described to viral vectors. Finally, the modular protein was found a versatile vehicle, being able to efficiently delivery different nucleic acids cargoes, including dsRNA, with an efficiency similar to that of the commercial vector Lipofectamine™ 2000.

Acknowledgement

The authors acknowledge the financial support of the Fundação de Amparo à Pesquisa do Estado de São Paulo – FAPESP (São Paulo, Brazil, grants 2012/18850-8 and 2013/23780-1) to ARA and the financial support of the Instituto Nacional de Investigación y Tecnología Agraria y Alimentaria INIA-Ministerio de Economía (grant RTA2012-00028-C02-02) to NFM. We appreciate the support of Cell Culture Unit of Servei de Cultius Cellulars, Producció d'Anticossos i Citometria (SCAC), and from Servei de Microscòpia, especially to Dr. Mónica Roldán for her technical advice, both at the UAB. We also acknowledge the ICTS "NANBIOSIS", more specifically to the Protein Production Platform of CIBER in Bioengineering, Biomaterials & Nanomedicine (CIBER-BBN)/IBB, at the UAB SepBioES scientific-technical service (http://www.nanbiosis.es/unit/u1-protein-production-platform-ppp/). The authors also appreciate the technical support of Amable Bernabé from Soft Materials Service (ICMAB-CSIC/CIBER-BBN). UU received a Sara Borrell post-doctoral fellowship from ISCIII, and AV an ICREA ACADEMIA award.

Conflict of interest

The authors declare no financial or commercial conflict of interest

5 References

[1] Naldini, L., Gene therapy returns to centre stage. *Nature* 2015, 526, 351–60. doi:10.1038/nature15818

[2] Bryant, L.M., Christopher, D.M., Giles, A.R., Hinderer, C. et al., Lessons learned from the clinical development and market authorization of Glybera. *Hum. Gene Ther. Clin. Dev.* 2013, 24, 55–64. doi:10.1089/humc.2013.087

[3] Morrison, C., $1-million price tag set for Glybera gene therapy. *Nat. Biotechnol.* 2015, 33, 217–8. doi:10.1038/nbt0315-217

[4] Negre, O., Bartholomae, C., Beuzard, Y., Cavazzana, M., et al., Preclinical Evaluation of Efficacy and Safety of an Improved Lentiviral Vector for the Treatment of -Thalassemia and Sickle Cell Disease. *Curr. Gene Ther.* 2015, 1, 64–81.

[5] Clement, N., Knop D. R., Byrne B. J. Large-scale adeno-associated viral vector production using a herpesvirus-based system enables manufacturing for clinical studies. *Hum. Gen. Ther.* 2010, 806, 796–806. doi: 10.1089/hum.2009.094

[6] Mingozzi, F., High, K.A., Review Article Immune responses to AAV vectors : overcoming barriers to successful gene therapy. *Blood* 2016, 122, 23–37. doi:10.1182/blood-2013-01-306647.

[7] Baldo, A., Van Den Akker, E., Bergmans, H.E., Lim, F., Pauwels, K., General Considerations on the Biosafety of Virus-derived Vectors Used in Gene Therapy and Vaccination. *Curr Gene Ther.* 2013, 13, 385–394. doi:10.2174/15665232113136660005

[8] Foldvari, M., Chen, D.W., Nafissi, N., Calderon, D. et al., Non-viral gene therapy: Gains and challenges of non-invasive administration methods. *J. Control. Release.* 2015, doi:10.1016/j.jconrel.2015.12.012

[9] Albanese, A., Tang, P.S., Chan, W.C.W., The Effect of Nanoparticle Size, Shape, and Surface Chemistry on Biological Systems. *Annu. Rev. Biomed. Eng.* 2012, 14, 1–16. doi:10.1146/annurev-bioeng-071811-150124

[10] Jiang, W., Kim, B.Y.S., Rutka, J.T., Chan, W.C.W., Nanoparticle-mediated cellular response is size-dependent. *Nat. Nanotechnol.* 2008, 3, 145–50. doi:10.1038/nnano.2008.30

[11] Petros, R. a, DeSimone, J.M., Strategies in the design of nanoparticles for therapeutic applications. *Nat. Rev. Drug Discov.* 2010, 9, 615–627. doi: 10.1038/Nrd2591

[12] MaHam, A., Tang, Z., Wu, H., Wang, J., Lin, Y., Protein-based nanomedicine platforms for drug delivery. *Small* 2009, 5, 1706–1721. doi:10.1002/smll.200801602

[13] Wang, T., Upponi, J.R., Torchilin, V.P., Design of multifunctional non-viral gene vectors to overcome physiological barriers: dilemmas and strategies. *Int. J. Pharm.* 2012, 427, 3–20. doi:10.1016/j.ijpharm.2011.07.013

[14] Toledo, M.A.S., Janissen, R., Favaro, M.T.P., Cotta, M.A., et al., Development of a recombinant fusion protein based on the dynein light chain LC8 for non-viral gene delivery. *J. Control. Release* 2012, 159, 222–231. doi:10.1016/j.jconrel.2012.01.011

[15] Toledo, M.A.S., Favaro, M.T.P., Alves, R.F., Santos, C.A., et al., Characterization of the human dynein light chain Rp3 and its use as a non-viral gene delivery vector. *Appl. Microbiol. Biotechnol.* 2014, 98, 3591–3602. doi:10.1007/s00253-013-5239-5

[16] Roberts, A.J., Kon, T., Knight, P.J., Sutoh, K., Burgess, S. A., Functions and mechanics of dynein motor proteins. *Nat. Rev. Mol. Cell Biol.* 2013, 14, 713–26. doi:10.1038/nrm3667

[17] Favaro, M.T.P., de Toledo, M.A.S., Alves, R.F., Santos, C.A. et al., Development of a non-viral gene delivery vector based on the dynein light chain Rp3 and the TAT peptide. *J. Biotechnol.* 2014, 173, 10–18. doi:10.1016/j.jbiotec.2014.01.001

[18] Wang, F., Wang, Y., Zhang, X., Zhang, W.,et al., Recent progress of cell-penetrating peptides as new carriers for intracellular cargo delivery. *J. Control. Release.* 2014, 174, 126–136. doi:10.1016/j.jconrel.2013.11.020

[19] Brock, R., The uptake of arginine-rich cell-penetrating peptides: Putting the puzzle together. *Bioconjug. Chem.* 2014, 25, 863–868. doi:10.1021/bc500017t

[20] Ben-Dov, N., Korenstein, R., The uptake of HIV Tat peptide proceeds via two pathways which differ from macropinocytosis. *Biochim. Biophys. Acta - Biomembr.* 2015, 1848, 869–877. doi:10.1016/j.bbamem.2014.12.015

[21] Schindelin, J., Arganda-carreras, I., Frise, E., Kaynig, V., et al., Fiji - an Open Source platform for biological image analysis. *Nat. Methods.* 2012, 9, 676-82 doi:10.1038/nmeth.2019.Fiji

[22] Hingorani, M.M., Donnell, M.O., Toroidal proteins : Running rings around DNA. *Curr. Biol.* 1998, 8, 83–86. doi: 10.1016/S0960-9822(98)70052-1

[23] Döhner, K., Nagel, C.-H., Sodeik, B., Viral stop-and-go along microtubules: taking a ride with dynein and kinesins. *Trends Microbiol.* 2005, 13, 320–7. doi:10.1016/j.tim.2005.05.010

[24] Cardarelli, F., Digiacomo, L., Marchini, C., Amici, A. et al., The intracellular trafficking mechanism of Lipofectamine-based transfection reagents and its implication for gene delivery. *Sci. Rep.* 2016, 6, 25879. doi:10.1038/srep25879

[25] Vighi, E., Montanari, M., Ruozi, B., Tosi, G., et al., Nuclear localization of cationic solid lipid nanoparticles containing Protamine as transfection promoter. *Eur. J. Pharm. Biopharm.* 2010, 76, 384–93. doi:10.1016/j.ejpb.2010.07.012

[26] Douglas, M.W., Diefenbach, R.J., Homa, F.L., Miranda-Saksena, M. et al., Herpes simplex virus type 1 capsid protein VP26 interacts with dynein light chains RP3 and Tctex1 and plays a role in retrograde cellular transport. *J. Biol. Chem.* 2004, 279, 28522–30. doi:10.1074/jbc.M311671200

[27] Lukacs, G.L., Haggie, P., Seksek, O., Lechardeur, D. et al., Size-dependent DNA Mobility in Cytoplasm and Nucleus *J. Biol. Chem.* 2000, 275, 1625–1629. doi: 10.1074/jbc.275.3.1625

[28] Suh, J., Wirtz, D., Hanes, J., Efficient active transport of gene nanocarriers to the cell nucleus. *Proc Natl Acad Sci U S A.* 2003, 100, 3878-82. doi: 10.1073/pnas.0636277100

[29] Radtke, K., Kieneke, D., Wolfstein, A., Michael, K., et al., Plus- and minus-end directed microtubule motors bind simultaneously to herpes simplex virus capsids using different inner tegument structures. *PLoS Pathog.* 2010, 6, e1000991. doi:10.1371/journal.ppat.1000991

[30] Smith, G.A., Gross, S.P., Enquist, L.W., Herpesviruses use bidirectional fast-axonal transport to spread in sensory neurons. *Proc Natl Acad Sci U S A.* 2001, 98, 3466-70. doi: 10.1073/pnas.061029798

[31] Ross, J.L., Shuman, H., Holzbaur, E.L.F., Goldman, Y.E., Kinesin and dynein-dynactin at intersecting microtubules: motor density affects dynein function. *Biophys. J.* 2008, 94, 3115–25. doi:10.1529/biophysj.107.120014

[32] Vázquez, E., Cubarsi, R., Unzueta, U., Roldán, M., et al., Internalization and kinetics of nuclear migration of protein-only, arginine-rich nanoparticles. *Biomaterials.* 2010, 31, 9333–9. doi:10.1016/j.biomaterials.2010.08.065

[33] Bausinger, R., von Gersdorff, K., Braeckmans, K., Ogris, M. et al., The Transport of Nanosized Gene Carriers Unraveled by Live-Cell Imaging. *Angew. Chemie* 2006, 118, 1598–1602. doi:10.1002/ange.200503021

[34] Ross, J.L., Wallace, K., Shuman, H., Goldman, Y.E., Holzbaur, E.L.F., Processive bidirectional motion of dynein-dynactin complexes in vitro. *Nat. Cell Biol.* 2006, 8, 562–70. doi:10.1038/ncb1421

Figure legends

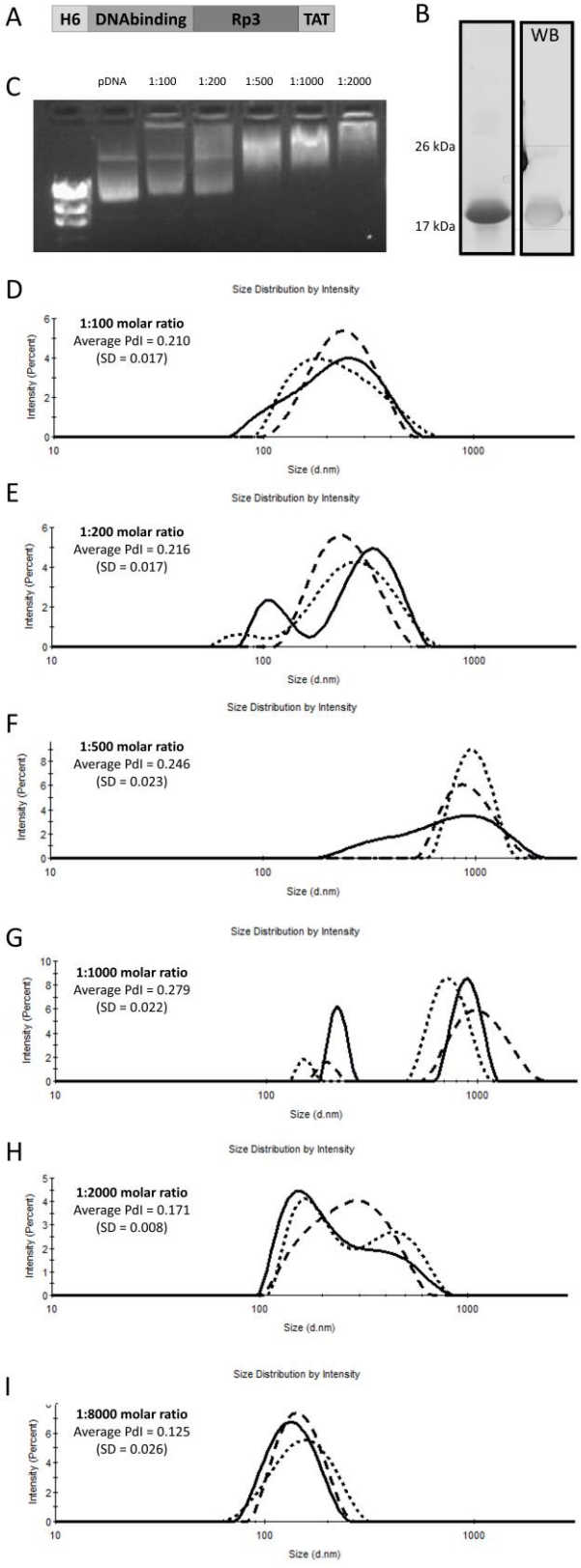

Figure 1. Characterization of the recombinant protein T-Rp3 regarding its ability to condense DNA. **(A)** Coomassie blue-stained sodium dodecyl sulfate polyacrylamide electrophoresis (Co) and HisTag-based Western Blot immunodetection (WB) of protein purified after *E. coli* expression. **(B)** Schematic representation of the modular protein T-Rp3. **(C)** Agarose gel retardation assay comparing increasing molar ratios of pDNA:T-Rp3, where molar ratios higher than 1:500 have the presence of shifted bands. **(D-I)** Dynamic light scattering results comparing the size distribution of particles formed in different molar ratios; first the size increases and then condensation effect takes place as size decreases with further addition of protein.

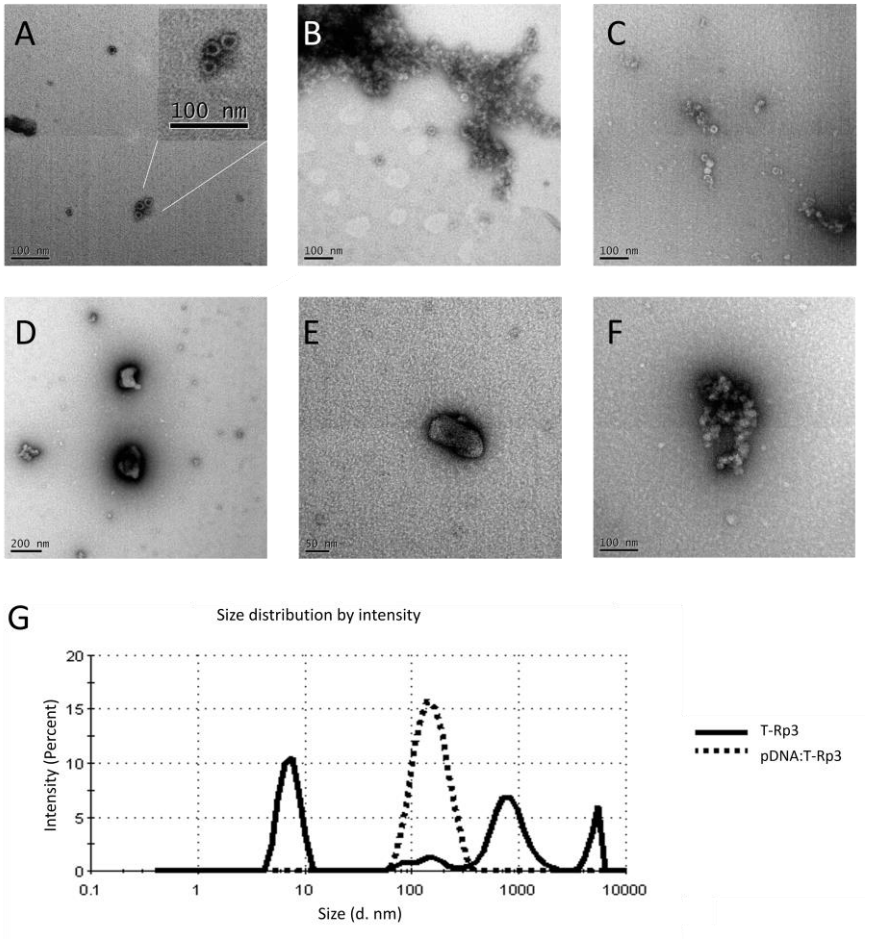

Figure 2. Evaluation of T-Rp3 behavior regarding size in the presence of pDNA. **(A-C)** Transmission electron microscopy (TEM) images of the protein self-assembled in small nanoparticles; while some aggregates are present, T-Rp3 is observed assuming a toroidal conformation. **(D-F)** Transmission electron microscopy images of the pDNA:T-Rp3, particles of globular shape, together with some smaller aggregates. **(G)** Dynamic light scattering results in agreement with TEM images, indicating that the addition of pDNA promotes an increase in size and reduction in polydispersity.

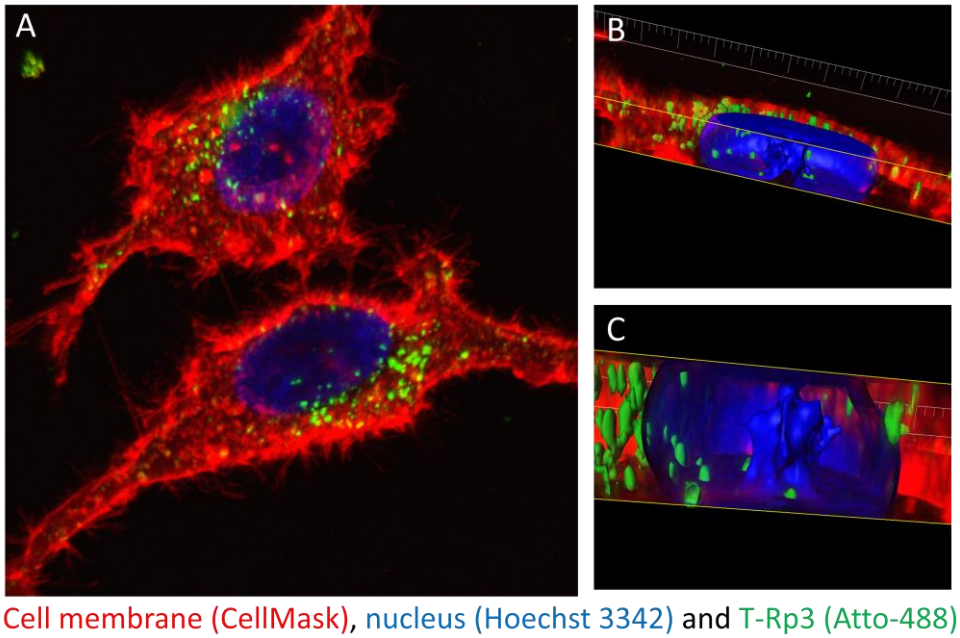

Figure 3. 3D LSCM images of live HeLa cells. **(A)** T-Rp3 (in green) is quickly internalized and accumulates in a specific area of the perinuclear region. **(B and C)** Sections of 3D reconstruction indicating that T-Rp3 is actually inside the cell, and as soon as 30 minutes post transfection, is attached to nuclear membrane, partially crossing it.

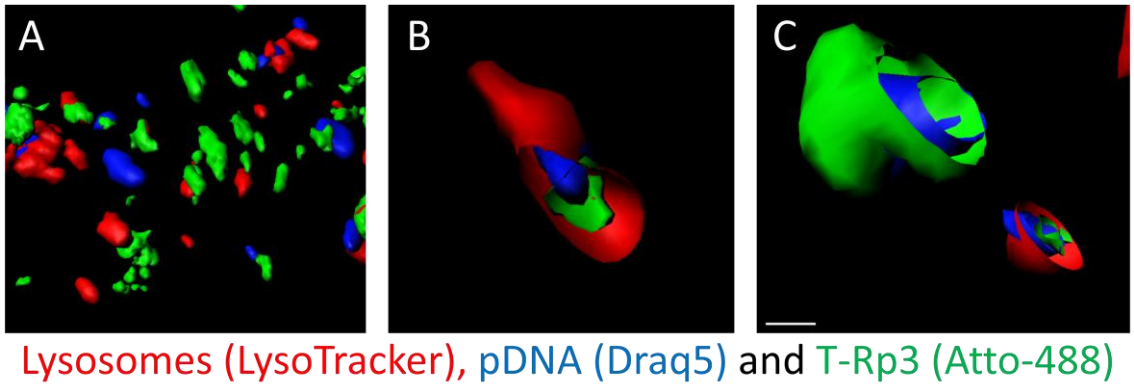

Figure 4. 3D LSCM images of live HeLa cells. **(A)** Lysosomes (red), pDNA (blue) and T-Rp3 (green) distribution inside the cells, where protein and pDNA can be observed inside lysosomes as well as free in the cytoplasm. **(B and C)** pDNA (blue) and T-Rp3 (green) observed attached together both inside and outside lysosomes (red). For further images please refer to the video available in the online version of the article.

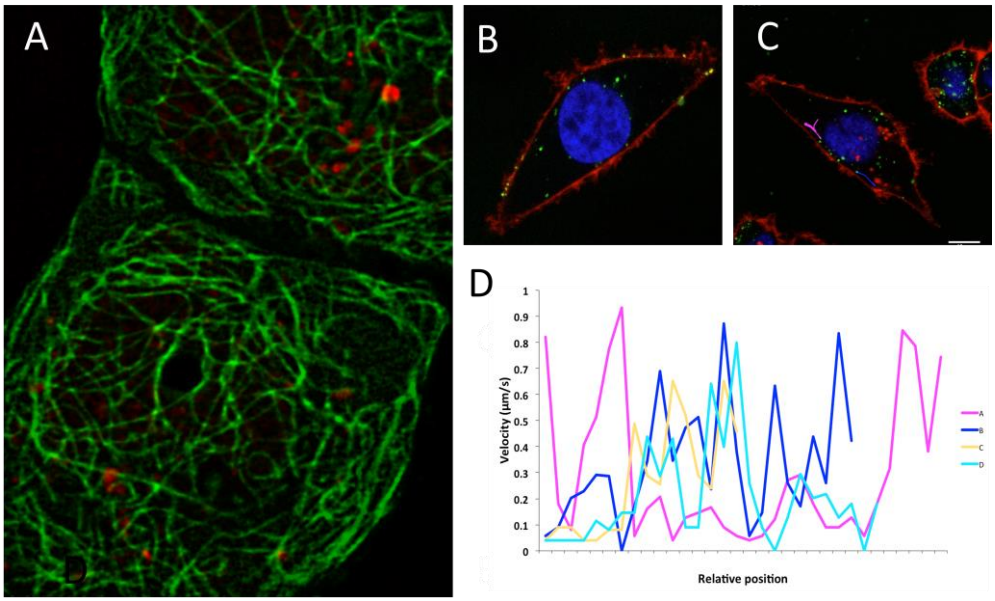

Figure 5. Assessment of T-Rp3 interaction with microtubules. **(A)** LSCM image showing pDNA (red) localization in relation to microtubules (green). **(B)** Within 30 minutes post transfection the protein (green) penetrates cellular membrane (colocalization with the membrane results in yellow dots) and reaches cytoplasm. **(C)** Still from the single particle tracking video (please refer to the video available in the online version) with the trajectory of two particles (pink and blue) highlighted **(D)** Analysis of the velocity of 4 individual fast-moving particles inside the cell.

Supplementary material - Figure 1. Assessment of the effect of Atto 488 and DRAQ5 on nanoparticle formation. **(A)** Dynamic light scattering results comparing the size distribution of particles, showing that Atto488 can promote a slight decrease in particle size, while the addition of DRAQ5 has no effect. **(B)** Transmission electron microscopy (TEM) images of the pDNA:T-Rp3-Atto 488 self-assembled in small nanoparticles.

Supplementary material - Video 1. Single particle tracking video showing T-Rp3 (in green) accumulating around the cell and soon being internalized to reach perinuclear region.

Supplementary material – Video 2. 3D LSCM images of live HeLa cells showing lysosomes (red), pDNA (blue) and T-Rp3 (green) distribution inside the cells, where protein and pDNA can be observed inside lysosomes as well as free in the cytoplasm. In the images pDNA and T-Rp3 are observed attached together both inside and outside lysosomes.

Supplementary material – Video 3. Single particle tracking video showing T-Rp3 (in green) traffic inside the cell. Four fast-moving particles were tracked and their trajectories where highlighted in colors.